In Situ Observation of Domain Structure in Monolayers of Arachidic Acid/γ-Fe_2O_3 Nanoparticle Complexes at the Air/Water Interface

Young Soo Kang,*,† Don Keun Lee,† and Choong Sub Lee‡

Department of Chemistry, Pukyong National University, Pusan 608-737, Korea

Pieter Stroeve

Department of Chemical Engineering and Materials Science, University of California, Davis, California 95616

Received: December 10, 2001; In Final Form: June 24, 2002

The Langmuir layer behavior of arachidic acid/γ-Fe_2O_3 nanoparticle complexes was studied at the air/water interface. The subphase was an aqueous colloidal solution (hydrosol) of γ-Fe_2O_3 nanoparticles with an average diameter of 8.3 nm and with a standard deviation of ±1.4 nm. Formation of the complex between arachidic acid and γ-Fe_2O_3 nanoparticles was studied with surface pressure−area isotherms, surface potential−area isotherms and Brewster angle microscopy. Increasing surface pressure resulted in a transition from well-separated domains of the complex to well-compressed, nanoparticulate layers and, ultimately, to multiparticulate layers. The magnetic nanoparticles and layers of nanoparticles on solid substrates were studied with FTIR, Mössbauer spectroscopy and vibrating sample magnetometry (VSM). The γ-Fe_2O_3 nanoparticles and Langmuir−Blodgett films with the nanoparticles showed superparamagnetic properties. The stability of the γ-Fe_2O_3 nanoparticle hydrosol solution was studied by ζ potential measurements. Positively charged γ-Fe_2O_3 nanoparticles in aqueous hydrosol solution at pH 3.5−5 showed excellent long-term colloidal stability.

Introduction

There has been growing interest in the synthesis of nanoscale inorganic materials, due to the novel properties exhibited by particles of very small dimensions. Materials such as CdS, TiO_2, γ-Fe_2O_3, and Fe_3O_4 have been widely studied. Cadmium sulfide and TiO_2 nanoparticles have excellent photocatalytic properties. Magnetic nanoparticles are of great interest for applications in information storage systems, catalysts, ferrofluids, and medical diagnostics.[1−6] Among magnetic particles, many studies have been devoted to nanoparticles of magnetite (Fe_3O_4) and maghemite (γ-Fe_2O_3). These iron oxides with sizes less than 10 nm have been synthesized in various matrix materials such as polymers,[7] micelles,[8] vesicles,[9] and lipid bilayer membranes.[10] Nanocomposites of organic materials and inorganic nanoparticles are of great promise as composites for utilization in high speed and high capacity optical and magnetic information storage media.[3,11] The focus of this study is to investigate the Langmuir behavior of nanocomposite monolayers, composed of arachidic acid and γ-Fe_2O_3 nanoparticles at the air/water interface, with pressure−area isotherms and surface potential−area isotherms. The in situ domain structure and molecular orientation of the complex were measured with Brewster angle microscopy (BAM).[12] The characterization of Langmuir−Blodgett (L−B) nanocomposite films was carried out with FTIR and UV−vis spectroscopy. The magnetic properties of the magnetic nanoparticles and the Langmuir−Blodgett films were characterized with vibrating sample magnetometry (VSM) and Mössbauer spectroscopy.

† Department of Chemistry.
‡ Department of Physics.

Experimental Section

Materials. The chemicals $FeCl_2 \cdot 4H_2O$ (99+%), $FeCl_3 \bullet 6H_2O$ (99+%), and arachidic acid (99+%) were obtained from Aldrich Chemical Co. and used without further purification. Distilled water was passed through a six-cartridge Barnstead Nanopure II purification train with a Macropure pretreatment. Organic solvents, such as chloroform and methanol, were either spectroanalyzed or HPLC grade.

Synthesis and Characterization of Iron Oxide Nanoparticles. Volumes of 0.28 mL of 11.5 N HCl and 8.3 mL of purified, deoxygenated water (resistance of 18 MΩ, by nitrogen gas bubbling for 30 min) were combined, and 2.86 g of $FeCl_3 \cdot 6H_2O$ and 1.00 g of $FeCl_2 \cdot 4H_2O$ were dissolved in the prepared solution with stirring for 20 min. The resulting solution was added dropwise into 100 mL of 1.5 M NaOH solution under vigorous stirring for 30 min. The precipitate was isolated in a magnetic field, and the supernatant was removed from the precipitate by decantation. A volume of 250 mL of purified water was added to the precipitate, and the solution was decanted after centrifugation at 5000 rpm for 10 min. After repeating the last procedure three times, 150 mL of 0.01 M HCl solution was added to the precipitate with stirring to neutralize the anionic charges on the nanoparticles. The clear hydrosol of γ-Fe_2O_3 at pH 3.5 was used as a subphase for Langmuir monolayers in a Langmuir trough. The concentration of hydrosol of γ-Fe_2O_3 was determined to be 9.29×10^{-5} M with an atomic absorption spectrophotometer (AAS Vario 6). The ζ potential of γ-Fe_2O_3 nanoparticles in an aqueous colloidal solution was measured with a Brookhaven Instrument Co. Model ZetaPlus. Transmission electron microscopy (TEM) experiments were carried out on a JEOL 200 CX transmission electron microscope. The TEM samples were prepared on 400 mesh copper grids coated with carbon that were purchased from Electron Microscope Co. A

10.1021/jp014484c CCC: $22.00
Published on Web 08/17/2002

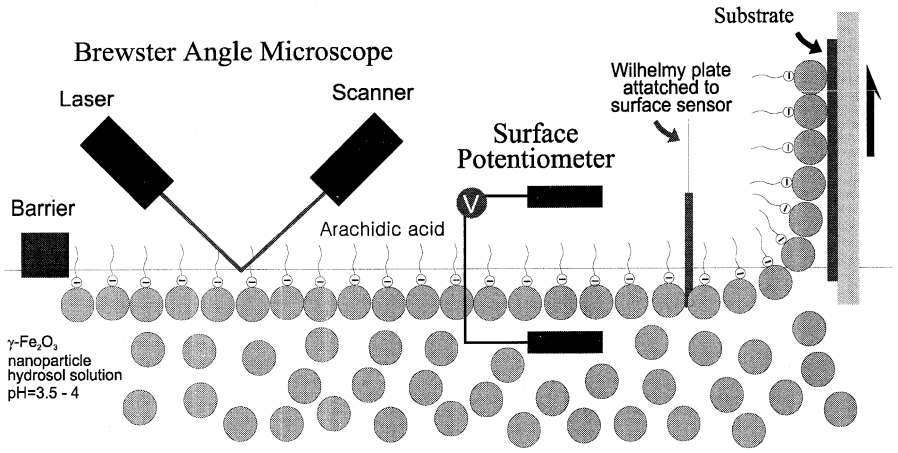

Figure 1. Schematic drawing of the Langmuir trough setup for both isotherm and Brewster angle microscopy experiments (775 mm × 12 mm, KSV 2000 System 3) housed within a large Plexiglas box to isolate it from the laboratory atmosphere.

drop of the stock solution was carefully placed on the copper grid surface and dried. Mössbauer spectra were recorded using a conventional Mössbauer spectrometer of the electromechanical type with a 20 mCi ^{57}Co source in an Rh matrix. To produce a uniform thickness over the area of the Mössbauer absorber, each sample was mixed with boron nitride powder. The area density of Fe for the flattened sample was 10 mg/cm^2. Optical absorption (UV−vis) and transmission FTIR spectra were recorded with a Varian CARY 1C UV−vis spectrophotometer and a Perkin-Elmer spectrum 2000, respectively. The magnetization curves and hysteresis loop of the nanocomposite L−B films were characterized with a Lake Shore Model 7300 VSM. The preparation of the nanocomposite L−B films were carried out by transferring Langmuir layers onto ZnSe and quartz plates, at a surface pressure of 20 mN/m, for FTIR and UV−vis optical absorption spectrophotometry analysis.

Pressure−Area Isotherms. The Langmuir trough for both the isotherm and BAM experiments (775 mm × 12 mm, KSV 2000 System 3) was housed within a large Plexiglas box to isolate it from the laboratory atmosphere, and the setup is shown in Figure 1. The setup included a surface pressure microbalance with a Wilhelmy plate. The KSV system was controlled by a PC-AT clone computer and KSV Film Control System Software (LB5000). Isotherm compression and data collection were automatically achieved through the use of computer software. Monolayer-spreading solutions (2 mM arachidic acid) were prepared by dissolving arachidic acid in chloroform. To spread a surface monolayer of a surfactant, a 60 μL aliquot of a spreading solution was delivered in different locations to the surface of the pure water subphase (or γ-Fe_2O_3 nanoparticle hydrosol solution at pH 3.5) at 20 °C with a Hamilton microliter syringe. The subphase temperature was controlled with a Jeio Tech Co. Ltd. refrigerated circulator, model RBC 20.

Surface Potential Measurement. The surface potential of the monolayer at the air/water interface was measured using the vibrating plate method (accuracy ±10 mV) with the surface potentiometer from KSV. The setup is shown in Figure 1. The surface potential−area (ΔV−A) isotherms of arachidic acid were measured for arachidic acid on the subphase of pure water and on 9.29×10^{-5} M γ-Fe_2O_3 nanoparticle hydrosols with the KSV 2000 surface potential measurement system at a temperature of 20 °C.

BAM Measurements. In the experimental setup of BAM (Nanofilm Tech., Germany) used for the characterization of monolayers and interfacial processes, the light beam of a pulsed laser (λ = 532 nm, beam diameter 1 mm) passed through a polarizer (set for p-polarization) was incident on the air/water interface at the Brewster angle (53.15°). The reflected beam was detected using a CCD camera. An image of the interface was formed through a microscope coupled to the CCD inclined at the Brewster angle, which collected the reflected light and a part of the light scattered by the interface. BAM images were recorded in situ with the NanoFilm Technology BAM 2 Plus on the KSV 2000 trough.

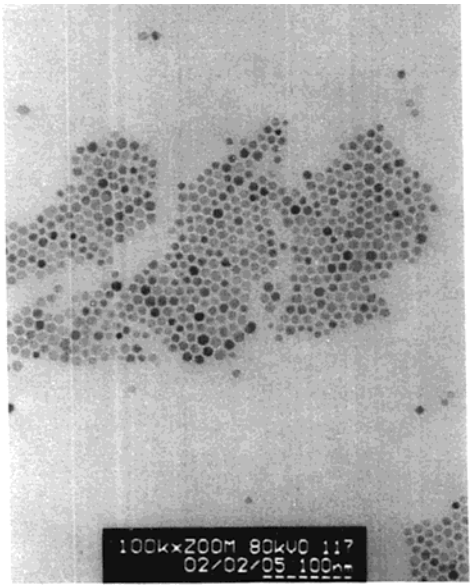

Figure 2. Transmission electron micrograph of γ-Fe_2O_3 nanoparticles. The average size is 8.3 ± 1.4 nm.

Results and Discussion

Average Size and the Study of Magnetic Property. The TEM image of γ-Fe_2O_3 nanoparticles, as shown in Figure 2, gave an average particle diameter of 8.3 nm with a standard deviation of ±1.4 nm. Because the hydrosol solution of the γ-Fe_2O_3 nanoparticle contains no surfactants, it can be used as a source for direct incorporation of the nanoparticles into ultrathin films with stearic acid without additional purification.

Bulk γ-Fe_2O_3 is ferrimagnetic at room temperature, but below a critical particle size it becomes superparamagnetic and shows no remanence or coercivity.[13−15] Figure 3 shows magnetization as a function of applied magnetic field of an arachidic acid/γ-Fe_2O_3 nanocomposite L−B film with 100 layers at room

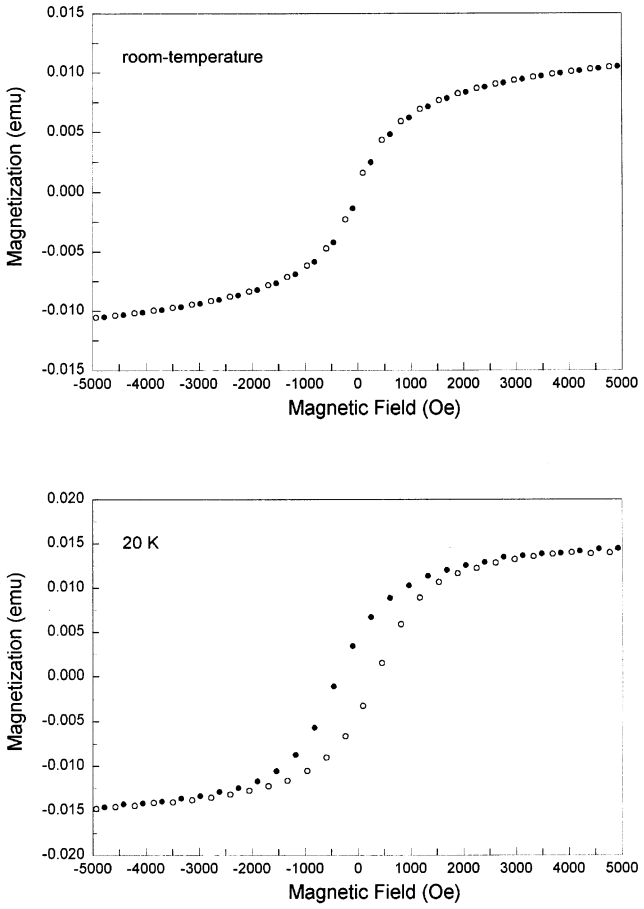

Figure 3. Magnetic hysteresis loop for a nanocomposite Langmuir−Blodgett film of arachidic acid/γ-Fe_2O_3 nanoparticles of 100 layers at room temperature. The lack of hysteresis indicates the composite has superparamagnetic properties (top). Magnetic hysteresis loop for a Langmuir−Blodgett film of arachidic acid/γ-Fe_2O_3 nanocomposite of 100 layers at 20 K. The presence of hysteresis at low temperature indicates that the γ-Fe_2O_3 nanoparticles undergo a superparamagnetic/single-domain transition (bottom).

temperature (top). No hysteresis at room temperature indicates superparamagnetic behavior. Below the blocking temperature, magnetic nanoclusters become magnetically frozen. The magnetic moment of the nanoclusters is fixed, and the remanence and coercivity in the hysteresis loop appear on the plot of magnetization as a function of the magnetic field.[13−16] Magnetization plots at 20 K are shown in the bottom of Figure 3. A small hysteresis loop appears, which has a 425 Oe coercivity with symmetric shape about the center.

The Mössbauer spectra of γ-Fe_2O_3 nanoparticles are shown in Figure 4. The Mössbauer spectra at room temperature and 77 K are fitted using the field distributions with the conditions that the line widths are fixed at 0.5 mm/s, the isomer shift and the quadrapole shift have the same value for each sextet, the magnetic hyperfine field range is 100−600 kOe in the step of 20 kOe and the intensity ratio is fixed at the theoretical ratio: 3.0:2.0:1.0. The vanishing quadrapole shift below the Neel temperature (T_N) comes from the summation of the quadrupole interactions for random distributions of the magnetic hyperfine field vector and the principal axes of the electric field gradient tensor. The spectrum at room temperature (top) consists of a sextet and a quadrupole doublet. The solid line through the data points is a sum of a sextet and a doublet subspectrum (given by the dotted lines). The presence of the quadrupole doublet means that the Neel temperature (T_N) of the magnetic particles

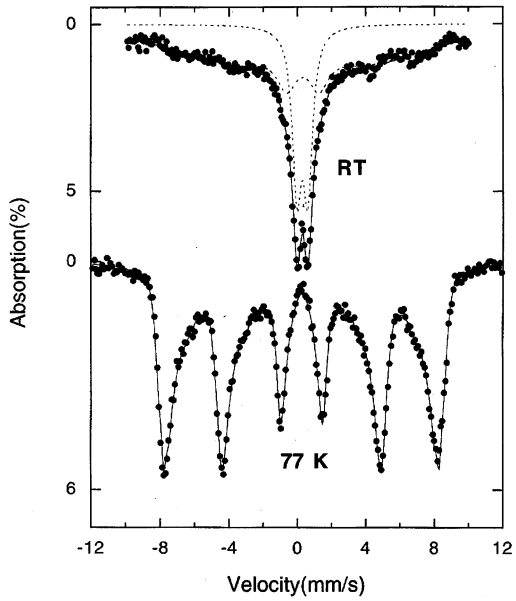

Figure 4. Computer-fitted Mössbauer spectra of γ-Fe_2O_3 nanoparticles at room temperature (top) and 77 K (bottom).

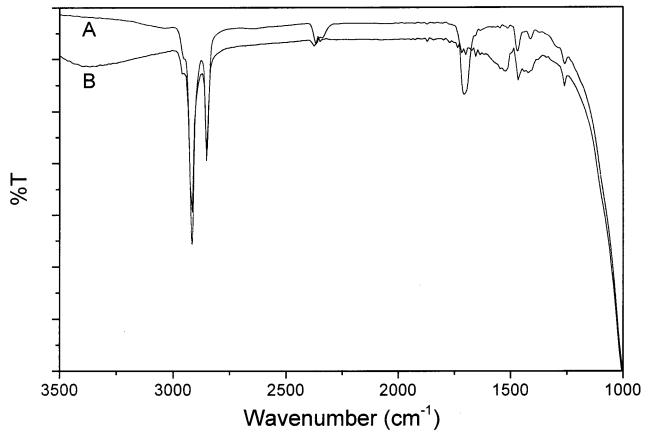

Figure 5. FTIR spectra of Langmuir−Blodgett films of arachidic acid deposited on a subphase of pure water (A) and on a hydrosol of γ-Fe_2O_3 nanoparticle (B), each with 25 layers.

is below the room temperature. The results show that the Neel temperatures (T_N) of nanometer-sized particles of magnetic materials are lower than those of bulk materials because of superparamagnetic phenomena.[17] The isomer shift of a quadrupole doublet at room temperature for γ-Fe_2O_3 is 0.30 ± 0.01 relative to Fe metal, which indicates ferric character.[18] The quadrupole splitting is 0.64 ± 0.01 mm/s and is due mostly to the valence and ligand contributions because the Fe^{3+} ions in γ-Fe_2O_3 occupy both the A- and B-site in iron-defect cubic spinel $(Fe)_A[\square_{1/3}Fe_{5/3}]_BO_4$. The ratio of the sextet is 76% of the total spectral area and the blocking temperature is above room temperature.[19]

FTIR and ζ Potentials. Figure 5 shows the FTIR spectra of L−B films of arachidic acid deposited from a subphase of pure water (A) and deposited from a hydrosol of γ-Fe_2O_3 at pH 3.5 (B). These samples were prepared with 25 L−B layers on ZnSe substrates at a surface pressure of 20 mN/m. The L−B film deposited from pure water shows an absorption peak around 1715 cm^{-1} (C═O stretching vibration band) for the carboxylic acid group. The L−B film deposited from the hydrosol of γ-Fe_2O_3 shows no absorption peak around 1715 cm^{-1} but shows a symmetric COO^- stretching vibration band at 1400 cm^{-1} and

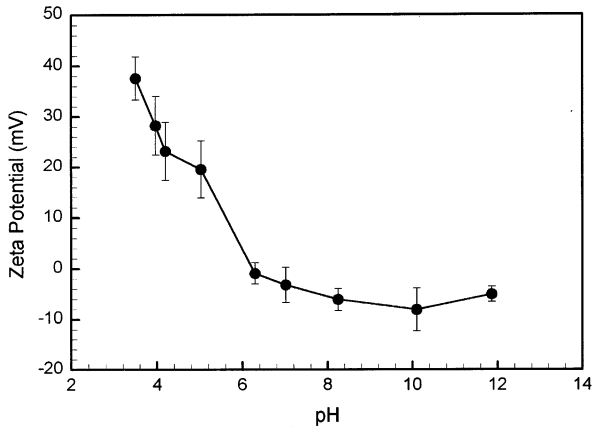

Figure 6. Dependence of ζ potential of γ-Fe_2O_3 nanoparticles on pH in aqueous colloidal solutions.

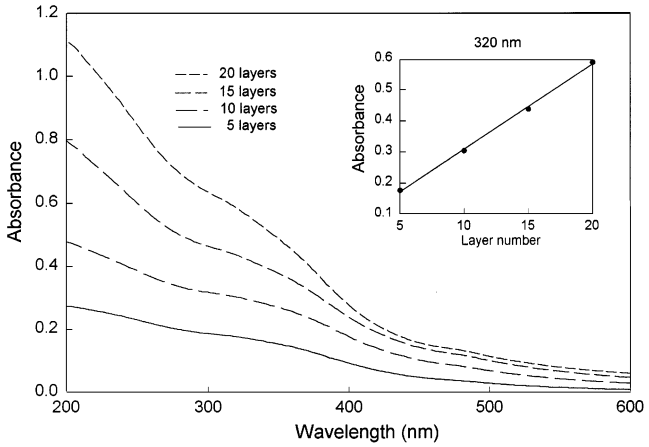

Figure 7. UV−vis spectra of an L−B film of arachidic acid/γ-Fe_2O_3 nanocomposite with 5, 10, 15, 25, and the optical absorbance versus the number of deposited layers at 320 nm.

an asymmetric COO^- stretching vibration band at 1525 cm^{-1}. The results suggest complexation of the positively charged γ-Fe_2O_3 nanoparticles with the carboxylates from the arachidic acid.

The surface charge of the iron oxide nanoparticle is positive in acidic solution less than pH 6.0, as determined by ζ potential measurements. The measurement of the ζ potential is often a key to understanding dispersion and aggregation processes of nanoparticles in hydrosol solutions. Figure 6 shows the dependence of the ζ potential of γ-Fe_2O_3 nanoparticles on pH in aqueous colloidal solutions. As expected for γ-Fe_2O_3 nanoparticles in the FTIR study, the ζ potential is positive at highly acidic pH values. The ζ potential decreases rapidly with increasing pH, becomes zero near pH 6, and then reaches a plateau region at pH 7−10. The consequence is that γ-Fe_2O_3 nanoparticles in hydrosol solution are very stable and dispersed at acidic pH because of the large positive charge, but at basic pH the nanoparticles become unstable and aggregated due to low values of the negative charge. The isoelectric point, that is the pH at which γ-Fe_2O_3 nanoparticles have a ζ potential of zero, is 5.8 ± 0.1.

UV−Vis Study. The UV−vis spectra and the optical absorption density versus the number of L−B layers of arachidic acid/γ-Fe_2O_3 nanoparticle films are shown in Figure 7. The spectra of L−B films deposited from a water subphase (i.e., without γ-Fe_2O_3 nanoparticles) did not show any absorption band. The spectra show a linear increase of optical absorption density around 320 nm with an increasing number of the layers in the

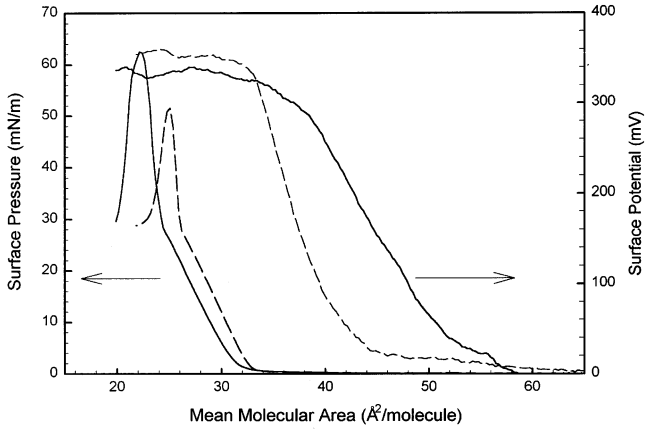

Figure 8. Surface pressure−area (left) and surface potential−area (right) isotherms of arachidic acid on a subphase of pure water (——) and on a hydrosol of γ-Fe_2O_3 nanoparticles (- - -) with pH 3.5 at 20 °C.

L−B films. The results indicate that the transfer ratio of the Langmuir monolayer at the air/water interface to the quartz plates is around 1.0. The linear increase of the optical absorption with the increasing number of deposited layers of the L−B films is consistent with a linear increase of the number of γ-Fe_2O_3 particles in the films. The linear increase is consistent with the linear increases of nanoparticles as measured with TEM and IR peak intensities of γ-Fe_2O_3 nanoparticle at 400, 450, 570, and 630 cm^{-1} (not shown).

Pressure−Area and Potential−Area Isotherms. Figure 8 shows the surface pressure−area isotherm (left) of arachidic acid on pure water (solid line) and on hydrosols of γ-Fe_2O_3 (dashed line). As the area is reduced, at first there is a coexistence between the gas and the liquid crystalline (L2) phases at very low surface pressures. The isotherm curves then show a typical continuous transition from a liquid tilted crystalline phase (L2 phase) to an untilted phase (the LS phase) at 28 mN/m.[25−28] The isotherm of arachidic acid on the hydrosol of γ-Fe_2O_3 is more expanded than that on pure water. The result suggests that the complexation of γ-Fe_2O_3 nanoparticles with the carboxylate groups of the arachidic acid expands the monolayer because the average diameter of the nanoparticles is much larger than the average distance between the carboxylate headgroups of the arachidic acid molecules.

The potential−area isotherms of arachidic acid on a subphase of pure water (solid line) and on a hydrosol of γ-Fe_2O_3 nanoparticle (dashed line) are also shown in Figure 8 (right). Both surface potential curves are saturated at about 33 $Å^2$ per molecule, which implies that above this specific area the alkyl tails of the arachidic acid on pure water and on a hydrosol of γ-Fe_2O_3 nanoparticles are beginning to tilt near the normal to the air/water interface, well before the isotherm curve begins to increase with surface pressure. The surface potential−area isotherm of arachidic acid on pure water is more expanded than on the hydrosol of γ-Fe_2O_3. A smoothly increasing surface potential curve of both systems confirms that stable Langmuir monolayers are formed around 28 mN/m surface pressure at the air/water interface (Figure 8).

BAM Study. The phase behavior of the arachidic acid monolayer on pure water (top) and on a hydrosol of γ-Fe_2O_3 nanoparticles (bottom) was observed with BAM, as shown in Figure 9. The arachidic acid monolayer is almost completely homogeneous, both on pure water and on a hydrosol of γ-Fe_2O_3 nanoparticles, in the coexisting tilted liquid crystalline−gaseous phase, as shown in Figure 9 A and B in the top and bottom

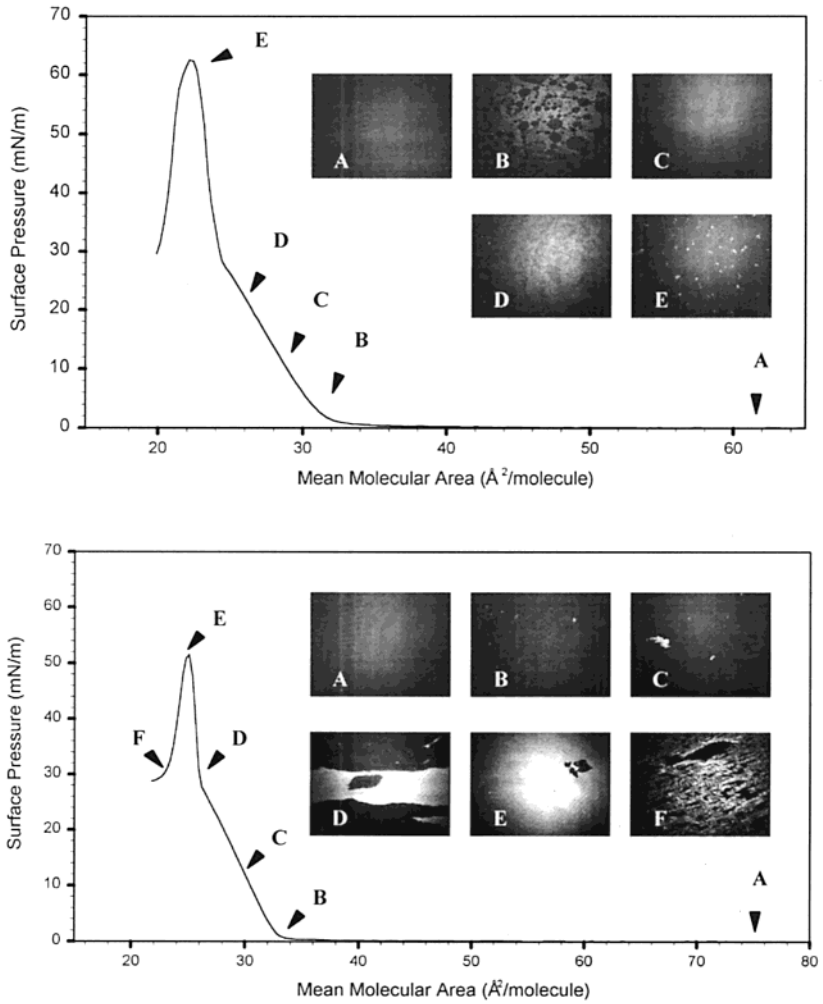

Figure 9. Pressure area isotherm and BAM images of arachidic acid on a subphase of pure water (top) and on a hydrosol of γ-Fe_2O_3 nanoparticles (bottom) with pH 3.5 at 20 °C.

panels. Further compression of the monolayer produces the images for the liquid crystalline phase of the monolayer on pure water, as shown in Figure 9 C and D in the top panel. In contrast to those results, additional compression of the arachidic acid monolayer on a hydrosol of γ-Fe_2O_3 nanoparticles results in the formation and growth of domains, as shown in Figure 9 D in the bottom panel. The results suggest the iron oxide particles are attached to the arachidic acid monolayer. Compression of the monolayer decreases the distance between the particles and increases the particle concentration. Because the nanoparticles have large sizes and refractive indexes, the association of the nanoparticles with the monolayer will probably dominate the BAM domain images at higher pressures and therefore better represent the behavior of the nanoparticles near the interface than of the fatty acid monolayer. As the particles come into closer proximity, there is an increase in the van der Waals attraction and in the electrostatic repulsion between the particles.[29] It is possible that because of size and charge, the nanoparticles cannot pack as closely as the fatty acid headgroups and perhaps arrange into multilayer regions. The growth of the size of the domain as a function of surface pressure in the pure water subphase and in the γ-Fe_2O_3 nanoparticles hydrosol subphase is reversible; upon reduction of the surface pressure, the domains decrease in size. In comparison, the arachidic acid monolayer without γ-Fe_2O_3 nanoparticles shows no domain formation except when the monolayer is collapsed. These domains are smaller in size than those observed with the hydrosol subphase.

Conclusions

Nanoparticles of γ-Fe_2O_3 were synthesized in an aqueous colloidal solution with an average diameter of 8.3 ± 1.4 nm. The ζ potential of γ-Fe_2O_3 nanoparticles in hydrosol solution is positive at acidic pH. The ζ potential decreases rapidly with pH and becomes zero at about pH 6, followed by a plateau region at pH 7−10. A positively charged surface of γ-Fe_2O_3 nanoparticles in aqueous hydrosol solution over pH 3.5−5 is consistent with the long-term colloid stability of these nanoparticles. Mössbauer and vibrating sample magnetometry spectra show that the γ-Fe_2O_3 nanoparticles and L−B films of the arachidic acid/γ-Fe_2O_3 nanocomposite have superparamagnetic properties. FTIR spectra of the L−B films show complexation of the positively charged γ-Fe_2O_3 nanoparticles with the carboxylates of the arachidic acid. A linear increase of optical absorption density around 320 nm with the deposition number of L−B layers indicates that the L−B deposition has a transfer ratio around 1.0. Surface pressure vs surface area isotherms and Brewster angle microscopy demonstrate that large surface pressures result in the formation and growth of domain structures probaly dominated by the aggregated state of γ-Fe_2O_3 nanoparticles in the monolayers at the air/water interface.

Acknowledgment. This work was supported by a Korea Research Foundation Grant (KRF-2000-015-DP0298).

References and Notes

(1) Charles, S. W.; Popplewell, J. In *Ferromagnetic Materials*; Wohlfarth, E. P., Ed.; North-Holland; Amsterdam, 1980; Vol. 2, p 509.

(2) Bate, G. *J. Appl. Phys.* **1981**, *52*, 2447.

(3) Ao, B.; Kummerl, L.; Haarer, D. *Adv. Mater.* **1995**, *7*, 496.

(4) Mallinson, J. C. *The Foundation of Magnetic Recording*; Academic: Berkeley, 1987; Chapter 3.

(5) Henglein, A. *Chem. Rev.* **1989**, *89*, 1861.

(6) Hadjipanayis G. C.; Prinz, G. A. *Science and Technology of Nanostructured Magnetic Materials*; Plenum: New York, 1991.

(7) (a) Ziolo, R. F.; Giannelis, E. P.; Weinstein, B. A.; O'Horo, M. P.; Ganguly, B. N.; Mehrotra, V.; Russell, M. W.; Huffman, D. R. *Science* **1992**, *257*, 219. (b) Butterworth: M. D.; Armes, S. P.; Simpson, A. W. *J. Chem. Soc., Chem. Commun.* **1994**, 2129. (c) Sohn, B. H.; Cohen, R. E. *Chem. Mater.* **1997**, *9*, 264.

(8) (a) Kommareddi, N. S.; Tata, M.; John, V. T.; McPherson, G. L.; Herman, M. F.; Lee, Y.-S.; O'Connor, C. J.; Akkara, J. A.; Kaplan, D. L. *Chem. Mater.* **1996**, *8*, 801. (b) Davies, K. J.; Wells, S.; Charles, S. W. *J. Magn. Mater.* **1993**, *122*, 24.

(9) Mann, S.; Sparks, H. C.; Board, R. G. *Adv. Microb. Physiol.* **1990**, *31*, 125.

(10) Zhao, X. K.; Herve, P. J.; Fendler, J. H. *J. Phys. Chem.* **1989**, *93*, 908.

(11) Zhao, X. K.; Horve, P. j.; Fendler, J. H. *J. Phys. Chem.* **1984**, *88*, 716.

(12) Liang, W.; Nakahara, H. *Chem. Lett.* **1984**, *88*, 716.

(13) Sohn, B. H.; Cohen, R. E. *Chem. Mater.* **1997**, *9*, 264.

(14) Vassiliou, J. K.; Mehrotra, V.; Russell, M. W.; Giannelis, E. P.; McMichael, R. D.; Shull, R. D.; Ziolo, R. F. *J. Apple. Phys.* **1993**, *73*, 5109.

(15) Kneller, E. In *Magnetism and Metallurgy*; Berkowitz, A. E., Kenller, E., Eds.; Academic Press Inc.: New York, 1969.

(16) Cullity, B. D. *Introduction to Magnetic Materials*; Addision-Wesley: Reading, MA, 1972.

(17) Zhao, J.; Huggins, F. E.; Feng, Z.; Huffman, G. P. *Phys. Rev. B* **1996**, *54*, 3403.

(18) Freeman, A. J.; Ellis, D. E. In *Mössbauer Isomer Shifts*; Shenoy, G. K., Wagner, F. E., Eds.; Amsterdam, New York, Oxford, 1978; Chapter 4.

(19) Mørup, S.; Bødker, F.; Hendriksen, P. V.; Linderoth, S. *Phys. Rev. B* **1995**, *52*, 287.

(20) Agathopoulos, S.; Nikolopoulos, P. *J. Biomed. Mater. Res.* **1995**, *29*, 421.

(21) Fowkes, F. M. *Ind. Eng. Chem.* **1964**, *56*, 40.

(22) Chattoraj,D. K.; Birdi, K. S. In *Adsorption and the Gibbs Surface Excess*; Plenum Press: New York, 1998.

(23) Allen, B. C. In *Liquid Metals*; Beer, S. Z., Ed.; Marcel Dekker: New York, 1972.

(24) Kang, Y. S.; Lee, D. K. Manuscript to be submitted to *Bull. Korean Chem. Soc*.

(25) Kaganer, V. M.; Möhwald, H.; Dutta, P. *Rev. Mod. Phys.* **1999**, *71*, 779.

(26) Dutta, P. *Colloids Surf. A: Physicochem. Eng. Aspects* **2000**, *171*, 59.

(27) Kaganer, V. M.; Peterson, I. R.; Kenn, R. M.; Shih, M. C.; Durbin, M.; Dutta, P. *J. Chem. Phys.* **1995**, *102*, 9412.

(28) Dutta, P.; Peng, J. B.; Lin, B.; Ketterson, J. B.; Georgopoulos, P.; Ehrlich, S. *Phys. Rev. Lett.* **1987**, *58*, 2228.

(29) Israelachvili, J. N. *Intermolecular and Surface Forces*; Academic Press: Orlando, FL, 1985.